Title

Estimating Evapotranspiration Using Semi-High Frequency Water Vapor Tracers

Author

Nguyen, Robin Khoa

Publication Date

2023

Peer reviewed|Thesis/dissertation

Estimating Evapotranspiration Using Semi-High Frequency Water Vapor Tracers

By

ROBIN KHOA NGUYEN
THESIS

Submitted in partial satisfaction of the requirements for the degree of

MASTER OF SCIENCE

in

Viticulture and Enology

in the

OFFICE OF GRADUATE STUDIES

of the

UNIVERSITY OF CALIFORNIA

DAVIS

Approved:

Megan Bartlett, Chair

Andrew McElrone

Mason Earles

Committee in Charge

2023

Abstract

Evapotranspiration (ET) is a critical variable in understanding soil-plant-atmosphere interactions and has been widely used as a parameter to inform irrigation. Common micrometeorological approaches to measuring ET are the Eddy Covariance (EC) and Surface Renewal (SR) methods; however, these methods are either not affordable, inaccessible, or rely on instrumentation that is too fragile to withstand environmental conditions and hinder agricultural operations. Like air temperature high-frequency time-series data, water vapor shows ramp-like patterns that can be used to estimate latent heat (LE) fluxes more directly. We applied a novel wavelet analysis to high-frequency (20 Hz) and semi-high frequency (1 Hz) water vapor data using a multilevel one-dimension wavelet decomposition based on the symlet wavelet to detect the amplitude and duration of ramp-like features over 30-minute intervals. The ET was computed based on this new method and compared to the EC and SR methods. ET estimates using the wavelet analysis approach strongly correlate with the estimates derived from EC and SR. Additionally, a more robust response at lower frequencies when using the wavelet analysis method suggests a more affordable, accessible, and direct method for estimating ET and offering growers a more cost-efficient and effective way to manage irrigation.

Acknowledgements

I would like to express my deepest gratitude to the following individuals and organizations who have played a significant role in my journey and the completion of this work. Their support, guidance, and encouragement have been invaluable.

First and foremost, I would like to thank my family and friends for their unwavering love and support throughout this entire endeavor. Their belief in me and constant encouragement have been instrumental in keeping me motivated and focused. I am truly grateful for their presence in my life.

I would also like to extend my appreciation to my 2023 Viticulture and Enology Cohort. The camaraderie and collaboration we shared have been integral to my personal and professional growth. It has been a privilege to learn alongside such a talented and passionate group of individuals.

Furthermore, I am deeply grateful to the Viticulture and Enology Faculty and Staff. Their expertise, mentorship, and dedication to fostering a conducive learning environment have been crucial in shaping my understanding of the field. I am indebted to their commitment to excellence and their willingness to go above and beyond to support their students.

A special mention goes to Andrew McElrone, Nico Bambach, and the rest of the McElrone Lab. Their guidance, expertise, and constant support have been pivotal in my research journey. Their enthusiasm for pushing the boundaries of knowledge in viticulture and enology is truly inspiring, and I am grateful for the opportunity to be a part of their team.

I would like to acknowledge the invaluable contributions of Kyaw Tha Paw U and Ian Faloona from UC Davis Atmospheric Science. Their expertise and insights in atmospheric science have greatly enhanced my understanding of this research project. Their commitment to

advancing atmospheric science has been instrumental in broadening my understanding of the complex interactions between grapevines and the environment.

I would also like to express my gratitude to the United States Department of Agriculture - Agricultural Research Service (USDA-ARS) for their financial support, which made this research possible. Their investment in scientific research is invaluable, and I am grateful for the opportunity to contribute to the advancement of knowledge in this field.

Table of Contents

1. Introduction

Evapotranspiration (ET) is a critical component of the hydrological cycle. ET is the combined process of transpiration through plant canopies and evaporation from soil, plants, and open water surfaces (Irmak, 2008; Miralles et al., 2020). Accurate estimation of ET, especially in irrigated agricultural systems, holds significant importance in facilitating efficient irrigation and water allocation plans while conserving the quantity and quality of available water sources worldwide (Irmak, 2008). Over the last century, remarkable progress in biometeorology has led to the development of reliable and precise methods for estimating ET, such as the eddy covariance (EC) and surface renewal (SR) methods (Paw U et al., 1992, 1995; Snyder et al., 1996; Baldocchi et al., 2001; Spano et al., 1997, 2002; Suvocarev et al., 2019). In this paper, we explore the development of these methods and observe a new alternative that can lead to a more affordable and reliable option for estimating ET.

1.1 The Fundamentals and Applications of EC

The EC methods rely on the movement of gaseous molecules driven by vortices called "eddies" in turbulent winds above the canopy, as shown in Figure 1 (Aubinet et al., 2012). The concentration of gaseous molecules (e.g., carbon dioxide or water vapor) and the wind speed are measured using a gas analyzer and a sonic anemometer, respectively. These instruments are mounted on a tower above the canopy. Ideally, the EC method works best under the following assumptions/conditions: (1) the ecosystem being studied is flat, (2) the environmental conditions are steady, and (3) the underlying vegetation of the ecosystem extends upwind for an extended distance (Baldocchi, 2003). Typically, the minimum surface area required for the EC method is approximately 50 to 100 times the effective measurement height (Aubinet et al., 2012). This ensures that EC measurements are taken in a well-adjusted boundary layer and are not affected

by any advection effects. In non-ideal ecosystems or very complex terrains, EC needs to account for atmospheric storage, flux divergence/convergence, and advection to minimize systematic errors (Baldocchi, 2003).

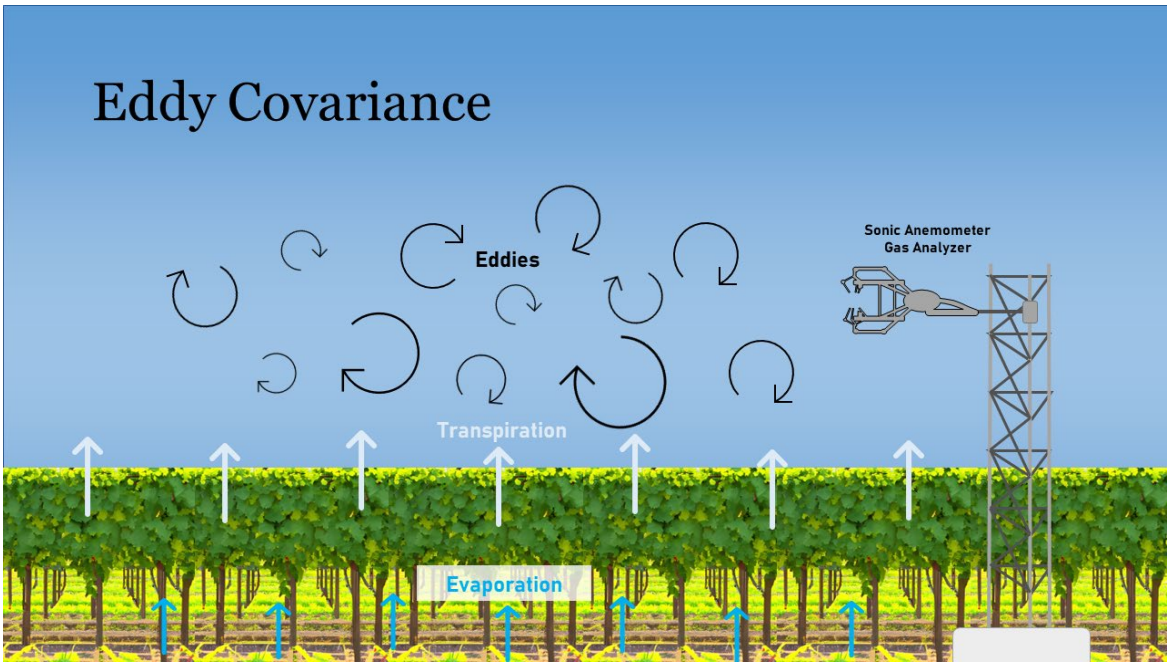

Figure 1 Illustration adapted from Aubinet et al. (2012) depicting a Schematic of vortices called "eddies" that are produced in turbulent winds above a canopy system.

Figure 2 illustrates the gas analyzer tracking the concentration changes of gas molecules as they are transported by eddies, while the sonic anemometer monitors fluctuations in vertical wind speeds. At time 1, eddy 1 moves air downwards with a concentration of gas, c_1, at a vertical wind speed of w_1. At time 2, eddy 2 moves air with a different concentration of gas, c_2, upwards at a vertical wind speed of w_2. The difference in gas concentration between these time periods indicates the flux of the gas of interest. Over time, the variations in upward and downward concentration changes allow us to determine the amount of that gas leaving the system.

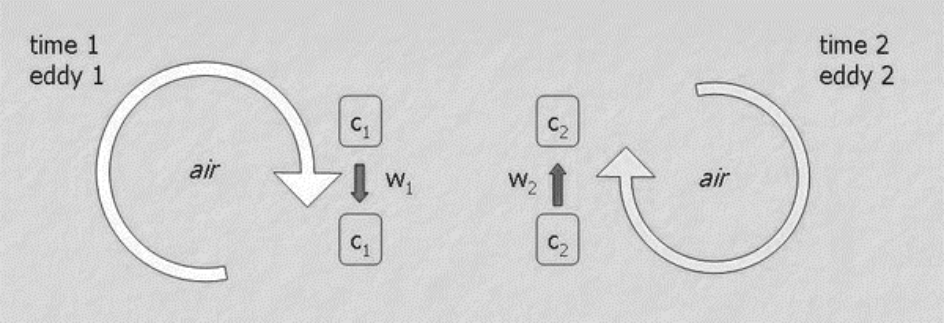

Figure 2 Theoretical depiction of eddies moving air parcels at two different time points (Burba, 2013).

Fundamentally, the EC method measures the instantaneous covariance between upward and downward motions of air and the concentration of gases contained within air parcels above the ecosystem of study (Aubinet et al., 2012). This is advantageous because measurements through this system can be representative of the entire canopy system instead of an individual plant. Additionally, the EC method can provide hourly, daily, seasonal, and/or annual flux data. The mathematical basis of EC is derived from the conservation of mass (Baldocchi, 1988). The rate of change of the mixing ratio of a gas molecule of interest (I) is balanced by the sum of the mean horizontal and vertical advection (II), the divergent and convergent turbulent fluxes (III), molecular diffusion (D), and the source or sink (S) (Baldocchi, 1988).

$$\frac{\partial \overline{\chi}}{\partial t} = \left(-\overline{u}\frac{\partial \overline{\chi}}{\partial x} - \overline{v}\frac{\partial \overline{\chi}}{\partial y} - \overline{w}\frac{\partial \overline{\chi}}{\partial z}\right) + \left(-\frac{\partial \overline{u'\chi'}}{\partial x} - \frac{\partial \overline{v'\chi'}}{\partial y} - \frac{\partial \overline{w'\chi'}}{\partial z}\right) + D + S \qquad (1)$$

$$(I) \qquad (II) \qquad (III)$$

The u, v, and w terms represent the three-directional components of wind speed. The bar represents the mean of the corresponding variable while the apostrophe denotes the fluctuation of the corresponding variable. In the EC method, certain assumptions simplify equation 1. First, it is assumed that the ecosystem being studied is flat, horizontal, and homogenous, meaning no advection effects. Second, it is assumed that there is no source or sink that would significantly

influence the flux within the observed controlled area. Lastly, the divergence or convergence of turbulent fluxes is assumed to be negligible. Applying these assumptions to equation (1) eliminates (I), (II), the x and y components of (III), and S, leading to equation (2).

$$\frac{\partial \overline{w'\chi'}}{\partial z} = D \tag{2}$$

Through integration with respect to height, z, and application of Reynolds decomposition, equation (2) turns into equation (3), which is the generalized form of the EC equation.

$$F = -(\overline{\rho_a})(\overline{w'\chi'}) \tag{3}$$

Here, F is the flux of the gas molecule of interest, ρ_a is the density of air, and $\overline{w'\chi'}$ is the covariance between the fluctuation of the vertical wind speed, w', and the fluctuation of the mixing ratio of the gas, χ'.

Despite this method being widely used to measure the flux between the ecosystem and the atmosphere, there are limitations in its application. Because the EC relies on the covariance between the vertical wind fluctuations and the concentration of the gas molecules, it is imperative to prevent any rotational distortions. Typically, sonic anemometers track wind speed in three dimensions (Verma, 1990). However, these instrumentations are quite expensive and require a lot of expertise to use and maintain (Paw U et al., 2005). High-frequency sensors that measure certain scalars, such as carbon dioxide and water vapor, can also be expensive, making EC less accessible and affordable (Spano et al., 2000). These limitations were the driving factors that led to the development of SR.

1.2 The Rise of Surface Renewal

The concept of surface renewal is based on the temperature changes of moving air parcels between the canopy/ecosystem of interest and the atmosphere (Paw U and Brunet, 1991; Paw U et al., 1992; Snyder and Paw U, 1993; Paw U et al., 1995). As shown in Figure 3, an air parcel

first moves down simultaneously into the canopy. This is followed by a gradual increase in the temperature of the air parcel. Once the air parcel reaches a certain temperature, it is ejected out of the canopy and replaced by another air parcel. This pattern repeats, showing coherent structures of asymmetric triangular patterns in the temperature data. Taylor (1958) was the first to observe the asymmetrical triangular patterns in the temperature scalar that illustrated a gradual increase followed by a sudden drop in temperature (Figure 3). Since then, these "saw-tooth" like patterns have been shown to be a common feature of temperature measurements in turbulent shear flows (Antonia et al., 1979).

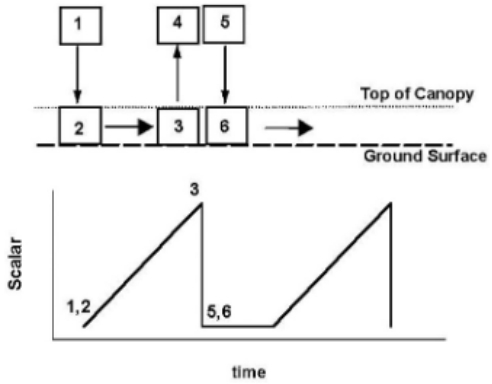

Figure 3. Schematic of the surface renewal method, illustrating the movement of air parcels and there corresponding changes in temperature over time measured at a single point above the canopy (Paw U et al., 2005).

The coherent structures' overall pattern can vary depending on the canopy and atmospheric conditions. In unstable conditions, the air above the canopy is cooler than within the canopy, leading to a warming effect as air parcels move down into the canopy, resulting in a rising ramp in the temperature data. Conversely, in stable conditions, the temperature patterns are reversed, with hotter air originating above the canopy and cooling as it moves down into the canopy, causing a decreasing ramp in the temperature data. Figure 4 illustrates stable and unstable conditions, represented by 'a' for amplitude, 's' for the quiescent period, and 'l' for the

period of gradually increasing (unstable conditions) or decreasing (stable conditions) temperature (Snyder et al., 1995).

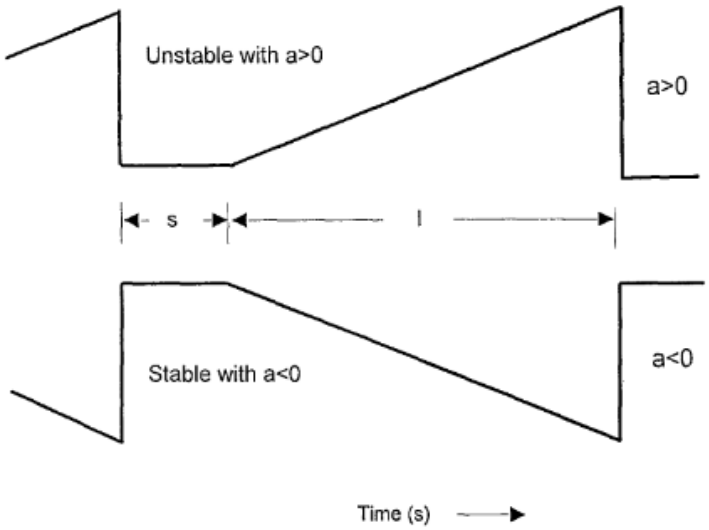

Figure 4. Illustration of the ramp-like features in temperature data for unstable and stable conditions over time. Here, the variable a represents the amplitude of the ramp, s represents the quiescent period, and l represents the period of gradual temperature increase (Snyder et al., 1995).

Despite the advantages of the SR method, there are certain limitations to this method. SR estimates have been shown to be inaccurate due to the uneven heating of air parcels (Paw U et al. 1995). To address the spatial temperature variations within air parcels, a calibration factor, α, is often calculated and applied to uncalibrated data obtained from SR. Various studies have demonstrated that α can vary depending on the crop being studied. Spano et al. (1997) indicated that α for grapevine canopies can range from 0.65 to 0.87, whereas for almond canopies, it can range from 0.27 to 0.59. Duce et al. (1997) found that grass, wheat, and sorghum may have α values around 1.0. This calibration is often achieved through linear regression forced at the origin between EC estimates and uncalibrated SR estimates (Paw U et al. 1995). As a result, SR

cannot function as a stand-alone method. It relies on EC estimations to provide more accurate and reliable data (McElrone, 2013). As previously mentioned, EC utilizes costly equipment that poses an economic barrier to estimating ET values.

Furthermore, commonly used equipment associated with SR, such as fine-wire thermocouples, poses a high risk of breakage. Research by Shapland et al. (2014) has shown that estimating ET using SR often involves the use of 13 μm and 76 μm diameter wires. However, these thin wires are susceptible to damage from natural elements like wind, rain, and even spider webs. Regular maintenance of the thermocouples is essential to prevent such damage and to ensure the reliability of temperature data above the canopy (McElrone, 2013). Replacing these delicate thermocouples can be challenging and might require specialized training due to the intricacies of working with extremely fragile sensors. While thermocouples themselves are not expensive, the frequent need for replacement can lead to a substantial long-term cost that may be difficult to manage. Thus, there is a need for other approaches to estimating ET.

1.3 Wavelet (WL) Analysis – An Alternative Method

The fundamental of the WL analysis is based on the Fourier Transform and windowed Fourier Transform (Chui, 1992). At its core, the Fourier Transform processes signals and decomposes them into a function of sines and cosines. It has practical uses in analyzing cellular signal communication, image processing, sound processing and filtering, electrical circuit designs, and many more (Kumar and Foufoula-Georgiou, 1994). However, the Fourier Transform has a huge disadvantage in providing only global information of an entire time series signal. With the Fourier Transform, frequency information can be extracted from time-series data, but the location and time information are lost. The windowed Fourier Transform observes a fixed time-frequency window, which offers more information on time-localization than the

Fourier Transform. However, the disadvantage to the windowed Fourier Transform is that it often overrepresents high-frequency information and underestimates low-frequency information (Lau and Weng, 1995).

The advantage of WL analysis is that it can obtain both localized frequency and time information of a given time-series. Mathematically, WL decomposes a signal in terms of some elementary function that can be stretched and translated to better fit the frequency patterns of the original signal of study (Lau and Weng, 1995). This flexibility allows WL to be scaled in such a way where extracting information on both high and low frequency signals is optimized. Generally, the decomposition of a signal using "daughter wavelets" from the translation and stretching of the "mother wavelet". Equation (4) is the general form of the product of this decomposition, where $\psi_{b,a}(t)$ is the resulting "daughter wavelet", a is the scaling factor, b is the translation factor, and $\psi(t)$ is the "mother wavelet" (Lau and Weng, 1995, Chui, 1992). As shown by Figure 5, there are many wavelet families that can act as the "mother wavelet" for WL of a signal.

$$\psi_{b,a}(t) = \frac{1}{(a)^{\frac{1}{2}}}\,\psi\left(\frac{t-b}{a}\right) \tag{4}$$

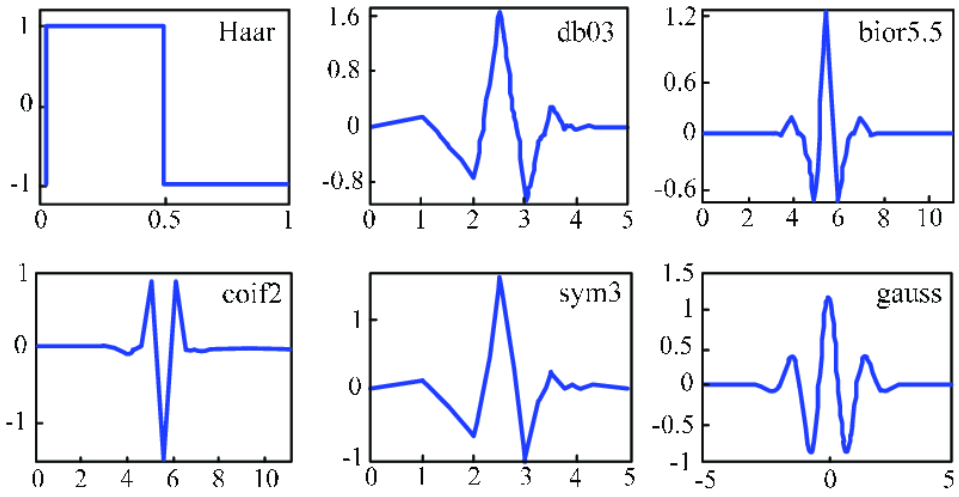

Figure 5. Illustration of different types of wavelet families (e.g., Haar, Daubechies, Biorthogonal, Coiflet, Symlet, Gaussian, etc.) and their general shape (López et al. 2017).

Decomposition of a signal utilizing WL requires convolution to produce wavelet coefficients, which involves taking the integral of the signal function multiplied by the wavelet of choice. This is as shown by equation (5), where $T(a,b)$ is the wavelet coefficient, $f(t)$ is the signal of study, and $\psi_{b,a}(t)$ is the "daughter wavelet" as represented by equation (4). With this decomposition using scalable daughter wavelets, the WL method could potentially more accurately capture the characteristics of ramp-like features as shown in temperature scalar data.

$$T(a,b) = \int_{-\infty}^{+\infty} f(t)\,\psi_{b,a}(t)\,dt \tag{5}$$

There are not many research studies that have applied WL in the field of bio micrometeorology, specifically in continuously processing surface turbulent fluxes. Multiple studies have used WL in observing coherent structures of turbulent motions above canopy systems like maize corn and forests (Brunet and Collineau, 1994; Thomas and Foken, 2005; Gao and Li, 1993). However, those studies have not been performed in long-term research monitoring surface turbulent fluxes from agricultural crops.

1.4 Purpose of Study

To increase the efficient use of water resources, it is imperative to have methods of measuring ET that are more accessible and affordable. Currently, many usages of the standard methods of estimating ET have been in the realm of academia and research. However, expanding the application of meteorological methods to estimate ET to common growers could increase efficient water usage and better preserve the limited water resources in many regions worldwide. As previously discussed, EC requires the use of sonic anemometer wind data, while SR requires calibration (often with EC data) and uses fragile thermocouples. These disadvantages can lead to financial barriers that prevent common growers from having the option to estimate ET within their own vineyards. Thus, this thesis explores WL as a new alternative method to estimating ET that circumvents these advantages (i.e., eliminate the necessity of wind data and a calibration factor). Additionally, this study also investigates the possibility of using water vapor data as the chosen scalar for ET estimations. Instrumentation for collecting water vapor data can be more durable and less expensive than thermal and sonic anemometer data; thus, supporting a more cost-effective option.

2. Materials and Methods

2.1 Vineyard Site Characteristics and Locations

This experiment centers around data from two vineyards that are part of the Grape Remote Sensing Atmospheric Profile and ET eXperiment (GRAPEX). The study focuses on a vineyard near Cloverdale, California, and a vineyard located near Madera, California, as illustrated in Figure 6. As detailed in Table 1, these vineyards differ in several aspects, including trellising systems, grape varieties, soil types, cover crops, and climatic profiles. Barrelli (BAR), established in 2010, mainly cultivates Cabernet Sauvignon. Its rows are oriented northeast-

southwest with approximately 3.35 meters of spacing between them. Situated in Sonoma County, the vineyard near Cloverdale experiences generally cooler temperatures due to its proximity to coastal regions, in contrast to the San Joaquin Valley vineyard (Madera). At Ripperdan (RIP), Chardonnay is the predominant variety grown. This site features narrower row spacing (2.74 meters apart) with an east-west orientation, distinguishing it from BAR. A detailed site description and agrometeorological conditions for these sites can be found in Bambach et al. 2022.

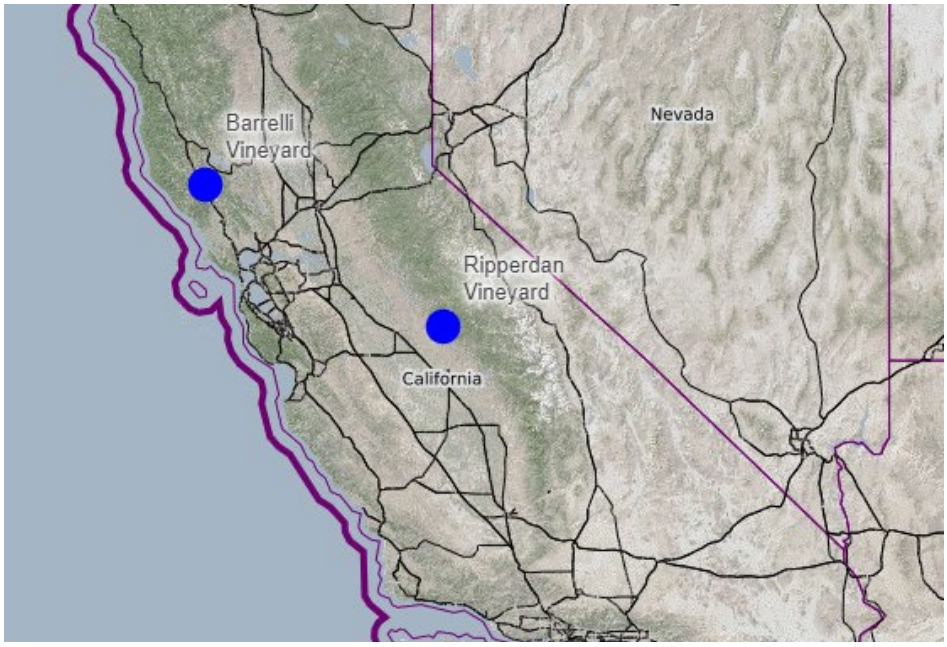

Figure 6. General Geographical Locations of Barrelli and Ripperdan vineyards near Cloverdale, CA and Madera, CA, respectively.

Table 1. Vineyard characteristics of Barrelli (BAR) and Ripperdan (RIP) that were studied.

	Barrelli Vineyard (BAR)	Ripperdan Vineyard (RIP)
Location	Sonoma County	San Joaquin Valley
Grape Variety Grown	Cabernet Sauvignon	Chardonnay and Merlot
Soil Type	Gravelly Loam	Sandy Loam

Trellising System	Elk Horn (Split Canopy)	Double Vertical
Cover Crop	Annual Mixed Grasses	Perennial Grasses
Row Spacing	3.35 meters	2.74 meters
Row Orientation	Northeast-Southwest	East-West
Canopy Height	2.2 meters	1.5-2.2 meters

The diverse array of trellising systems, climatic profiles, grape varieties, soil types, cover crops, and other factors represented by these two vineyard sites presents an invaluable opportunity for analyzing the robustness of the methods. Ensuring dependable ET estimation across a range of vineyards is significant. Therefore, by implementing EC, SR, and WL at these two distinct vineyard sites, we can gain valuable insights into their performance across various vineyard environments.

2.2 Instrumentation and Data Collection

Semi-high frequency water vapor tracers were measured above the canopy at each of the vineyard sites using Campbell Scientific's IRGASON®. The IRGASON® includes a sonic anemometer for wind speed and direction measurements (Ux (m/s), Uy (m/s), and Uw (m/s)) with a precision of 1 mm/s for Ux and Uy, and 0.5 mm/s for Uw. Additionally, it features an infrared gas analyzer for measuring H_2O Density (g/m^3). The open-path analyzer has a path length of 15.37 cm, providing a precision of 0.004 g/m^3. This instrument was mounted onto a flux tower at a height of approximately 4.8 meters from the ground and collected data at a frequency of 20 Hz throughout the year 2022. All data are stored in a CR6 Campbell Scientific Datalogger.

2.3 Data Processing

2.3.1 Data Cleaning

Raw water vapor density data, recorded at 20 Hz, underwent a quality control and spike removal process prior to applying EC, WL, and SR analyses. To mitigate spikes in water vapor density measurements, a rolling average method was performed using a window size of 600 observations. Further preprocessing involved identifying spurious data within the raw water vapor density data by calculating the difference between consecutive data points. Any observations with a difference exceeding 1.5 g/m^3 were deemed to be spurious data and subsequently eliminated from the raw dataset.

2.3.2 Methods of Estimating ET

EC, SR, and WL models were all applied to the cleaned water vapor density tracers at 20 Hz to produce ET estimations at every 30-minute interval. It is important to acknowledge that all the methods of estimation are applied to the same data collected using the infrared gas analyzer and sonic anemometer. ET estimated using EC at every 30-minute interval were calculated using equation (6), where w' and $\rho_{H2O}{}'$ represents the variance of vertical wind speed and water vapor density, respectively. The SR method estimates ET as defined by equation (7), where $\frac{d\rho_{WV}}{dt}$ is the water vapor density over time and V/A is the volume of air per unit area under the canopy height.

$$ET_{EC} = \overline{w'\rho_{H2O}{}'} \tag{6}$$

$$ET = \frac{d\rho_{WV}}{dt}\frac{V}{A} \tag{7}$$

It is assumed that the water vapor change over time ($\frac{d\rho_{WV}}{dt}$) can be replaced by the slope of the ramp-like features (a/l) in the water vapor data. Multiplying the expression by the relative time for heating ($l/(l+s)$), $\frac{d\rho_{WV}}{dt}$ gets replaced by $\frac{a}{l+s}$. The volume of air per unit area simplifies to z_c, the height of the canopy. Snyder et al. (1996), included an alpha term, α, to represent the calibration factor that accounts for the uneven heating from the bottom of the air parcel to the top. Applying all the modifications yields equation (8), where α is the calibration factor, $\frac{a}{l+s}$ is the slope of the ramp-like structures, and z_c is the height of the canopy.

$$ET = \alpha \frac{a}{l+s} z_c \tag{8}$$

Empirical calculations of the calibration factor follow the same method as found in Paw U et al. (1995) and Snyder et al. (1996), where α is the slope of the linear regression forced at the origin between EC estimates and uncalibrated SR estimates.

The slope ($\frac{a}{l+s}$) is estimated using the structure functions as outlined by Van Atta (1977). These structure functions capture the second, third, and fifth moments of the temperature data as shown by equations (9), (10), and (11), respectively.

$$\overline{S^2(r)_c} = \frac{a^2 r}{(l+s)}\left[1 - \frac{1}{3}\left(\frac{r}{l}\right)^2\right] \tag{9}$$

$$\overline{S^3(r)_c} = \frac{a^3 r}{(l+s)}\left[-1 + \frac{3}{2}\frac{r}{l} - \frac{1}{2}\left(\frac{r}{l}\right)^3\right] \tag{10}$$

$$\overline{S^5(r)_c} = \frac{a^5 r}{(l+s)}\left[-1 + \frac{5}{2}\frac{r}{l} - \frac{10}{3}\left(\frac{r}{l}\right)^2 + \frac{5}{2}\left(\frac{r}{d}\right)^3 - \frac{2}{3}\left(\frac{r}{l}\right)^5\right] \tag{11}$$

Utilizing these structure functions, *a* and *l+s* can be calculated by using equations (12) and (13), respectively.

$$0 = a^3 + \left[10\,\overline{S^2(r)_c} - \frac{\overline{S^5(r)_c}}{\overline{S^3(r)_c}}\right] a + 10\,\overline{S^3(r)_c} \tag{12}$$

$$(l+s) = -\frac{a^3 r}{\overline{S^3(r)_c}} \tag{13}$$

The Wavelet Transform (WL) method employs Discrete Wavelet Transform (DWT) to estimate ET. In the application of DWT, a set of discrete functions is convolved to modify the translational and dilation parameters in the mother wavelet, as represented by equation (4). This process generates daughter signals that are subsequently applied to the data. A multilevel 1D decomposition was executed using the "wavedec" function from the "pywavelet" package on the 20 Hz water vapor density time-series. This decomposition yields both approximation and detail coefficients, which are used to compute the duration and amplitude, respectively, of the ramp-like features within the water vapor density time-series over 30-minute intervals. As previously shown in Figure 5, there are many wavelet families that can be used to execute this decomposition for the approximate and detail coefficients; however, for this study, families that are good representation of the ramp-like features in the water vapor data are chosen. The Daubechies and Symlet wavelet families exhibit great representation based on visual observations. Despite their similarities, there was greater alignment with the Symlet family, particularly symlet 3, resulting in the implementation of WL using symlet 3 with five coefficients.

2.3.3 Surface Renewal Calibration Factor

The calibration factor, α, is often calculated by performing a linear regression forced at the origin between the uncalibrated estimations from SR and estimations from EC as outlined in multiple studies (Paw U et al., 1995; Spano et al., 1997). Adjusted SR estimations were obtained by multiplying α by the uncalibrated estimations from SR yields, as shown in equation (14).

$$ET_{SR} = \alpha\, ET_{SR(uncalibrated)} \tag{14}$$

2.3.4 Software

All data processing was conducted using Jupyter Notebook version 6.4.8, using a range of packages as summarized in Table 2. To derive ET estimates, functions corresponding to EC, WL, and SR were established within Jupyter Notebook, aligning with the equations presented in the theory section. After their formulation, these functions were then applied to the water vapor data to generate ET estimates for 30-minute intervals across each day of the year.

Table 2 List of Jupyter Notebook packages that were used to process and analyze semi-high frequency water vapor tracers.

Jupyter Notebook Package	Description
Datetime	Converted the datetime format from the raw data into a more useful format.
Csv	Read CSV files and transformed the raw data into a workable dataframe. Allowed to safe processed data into a CSV file.
NumPy	Used for multi-dimensional arrays and matrices and mathematical functions.
Pandas	Used for data manipulation and analysis
Matplotlib	Used for data plotting and visualization
pywt	Used for wavelet transforms and wavelet analysis

2.4 Data Analysis

The data analysis aims to assess the correlations between ET estimates obtained from EC, SR, and WL. This examination will provide insights into the performance of WL in comparison to EC (considered the benchmark research method) and SR. Furthermore, the data analysis also seeks to evaluate the robustness of these methods. As previously mentioned, the selection of vineyards characterized by diverse growth and climatic conditions serves to investigate the methods' efficacy under challenging circumstances. The overarching schematic of the data analysis is illustrated in Figure 7.

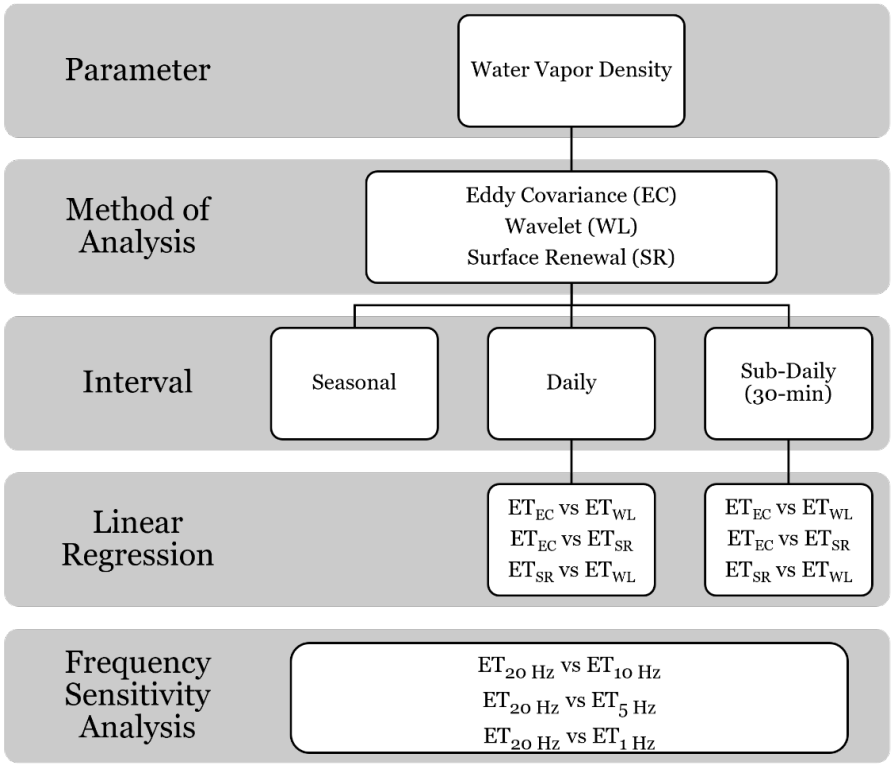

Figure 7. Schematic of data analysis.

2.4.1 Cook's Distance - Outlier Determination

Cook's Distance was used to identify data point that are potential outliers when performing a least-squares linear regression analysis (Cook, 1977). Cook's distance was calculated using equation (15), where D_i represents the sum of all changes in the regression when observation i is removed, $\hat{y}_j$ is the original regression, $\hat{y}_{j(i)}$ is the regression with observation i removed, p is the rank of the model, and s^2 is the mean squared error of the model. A point was identified as a potential outlier if D_i was above the threshold as shown in equation (16), where n is the total number of data points in the least-squared linear regression. While Cook's Distance is a useful tool at identifying potential outliers, it does not provide enough information to determine if the data point is valid (Fox, 1991). Further investigation of the data point was needed to determine if the data point is influenced by spurious data. Any spurious data were removed and not considered in the data analysis.

$$D_i = \frac{\sum_{j=1}^{n}\left(\hat{y}_j - \hat{y}_{j(i)}\right)^2}{ps^2} \tag{15}$$

$$Threshold = \frac{4}{n} \tag{16}$$

2.4.2 Least-Squares Linear Regression – Method Comparisons

Linear regressions were performed to compare ET estimations derived from each of the methods (EC, WL, and SR) at the sub-daily and daily levels. ET_{WL} was compared to ET_{EC} to determine the performance and validity of WL. ET_{SR} were compared to ET_{EC} to determine the efficacy of the SR method applied to water vapor data. ET_{WL} estimations were compared to ET_{SR} to verify if these two methods produce similar results. For each linear regression plot, the coefficient of determination, R^2, the slope of the linear equation, and the root mean squared error

(RMSE) were analyzed to determine the strength and direction of the correlation between the comparisons.

2.4.3 Frequency Sensitivity Analysis

The instruments used in this study gather data at a frequency of 20 Hz. Equipment operating at this frequency is generally more expensive than those collecting data at half or a quarter of that frequency. Given the study's focus on exploring a cost-effective alternative method, it becomes pivotal to apply WL and SR to lower frequency data and assess their performance. To achieve this, water vapor data at frequencies of 10 Hz, 5 Hz, and 1 Hz were extracted from the original 20 Hz dataset. These subsets were then utilized to estimate ET using WL and SR. Linear regressions were conducted to analyze the correlations in the following comparisons: 20 Hz vs 10 Hz, 20 Hz vs 5 Hz, and 20 Hz vs 1 Hz. Like previous analyses, the strength and direction of correlation were determined based on the coefficient of determination, R^2, the slope of the linear equation, and the root mean squared error (RMSE).

2.4.4 Root Mean Square Error Analysis

Root Mean Square Error (RMSE) was used to further evaluate the regression model within the least-squares linear regression, comparing the ET values obtained through the three estimation methods with those of the least-squares linear regressions in the frequency sensitivity analysis. RMSE values indicate the average difference between the predicted values from the regression model and the observed values and is calculated using equation (18), where P_i is the predicted value from the regression model, O_i is the observed value, and n is the total number of data points.

$$RMSE = \sqrt{\frac{\sum(P_i - O_i)^2}{n}} \tag{18}$$

Higher RMSE values in regression models indicate that, on average, the observed values are further from the predicted values of the model. Conversely, lower RMSE values in regression models indicate that, on average, the observed values are closer to the predicted values of the model.

3. Results

3.1 SR Alpha Calibration

Calibration was applied to the ET measurements from SR to address the nonuniform heating within the air parcel. As depicted in Figure 8, performing a least squares regression of $ET_{SR\ (uncalibrated)}$ against ET_{EC} resulted in α values of 0.631 and 0.504 for BAR and RIP, respectively. Notably, these α values for both vineyards are within range to those reported for grapevines studied by Spano et al. (1997) and for grass, wheat, and sorghum studied by Duce et al. (1997). Despite the higher average distance from the regression line for RIP's linear regression (RMSE = 0.036) in contrast to BAR's linear regression (RMSE = 0.047), the R^2 value show a strong correlation between $ET_{SR\ (uncalibrated)}$ and ET_{EC}.

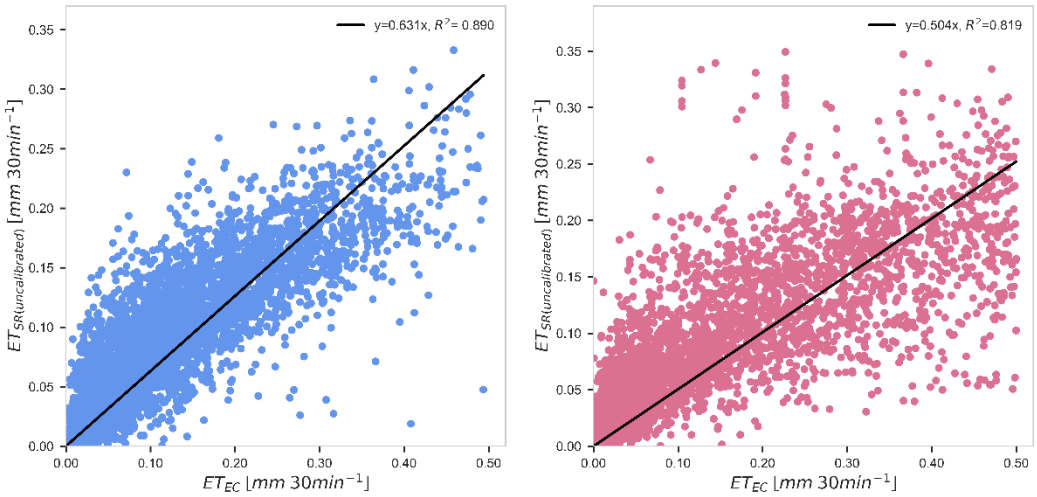

Figure 8. Linear regression between $ET_{SR\ (uncalibrated)}$ and ET_{EC} through the origin for the determination of the calibration factor, α. Blue points represent the 2022 data from BAR Vineyards. Pink points represent the 2022 data from RIP.

3.2 Comparison between ET_{WL}, ET_{EC}, and ET_{SR}

Sub-daily ET comparisons among EC, SR, and WL exhibited strong agreement in measuring evapotranspiration through 20 Hz water vapor density tracers at both the BAR and RIP sites. Cook's Distance outlier detection resulted in the removal of 8.57%, 10.90%, 10.87%, 8.89%, 10.33%, and 11.85% of data from ET_{EC} vs ET_{WL} (BAR), ET_{EC} vs ET_{SR} (BAR), ET_{WL} vs ET_{SR} (BAR), ET_{EC} vs ET_{WL} (RIP), ET_{EC} vs ET_{SR} (RIP), and ET_{WL} vs ET_{SR} (RIP), respectively. Further investigation confirmed these potential outliers as anomalies caused by condensation, adverse weather conditions, or human error during maintenance, warranting their exclusion from the data analysis. The removal of outliers resulted in enhanced R^2 values in the linear regression. Specifically, for the BAR vineyard site, the least-squares regression indicated a weaker correlation between ET_{EC} vs ET_{SR} ($R^2 = 0.775$) compared to the other two models – ET_{EC} vs ET_{WL} ($R^2 = 0.861$) and ET_{WL} vs ET_{SR} ($R^2 = 0.832$). Similarly, for RIP, ET_{EC} vs ET_{SR} also displayed a weaker correlation ($R^2 = 0.748$) compared to the other two models. Nevertheless, the

differences in R^2 between the comparisons for both vineyards were marginal. Looking at the RMSE (as presented in Table 3), estimations derived in each of the comparisons were not significantly different from each other. There were greater deviations among the BAR vineyard compared to the RIP vineyard, but the values are still comparable.

Based on the slopes of the linear regressions, the linear relationships between WL, SR, and EC are close to 1, demonstrating close estimations between the three methods. For RIP vineyards, WL slightly overestimates the ET values when compared to EC estimations, where the slope is equal is 1.2305. SR appears to underestimate the ET values when compared to EC estimations, where the slope is equal to 0.8287 and 0.9144, respectively.

Table 3. R-squared and root mean square error (RMSE) values for Linear Regression Models comparing sub- daily evapotranspiration estimations using Eddy covariance (EC), Surface Renewal (SR), and Wavelet Analysis (WL).

Vineyard Site	Comparison	R^2	RMSE
BAR	EC vs WL	0.861	0.021
	EC vs SR	0.775	0.023
	WL vs SR	0.832	0.023
RIP	EC vs WL	0.849	0.035
	EC vs SR	0.748	0.035
	WL vs SR	0.909	0.028

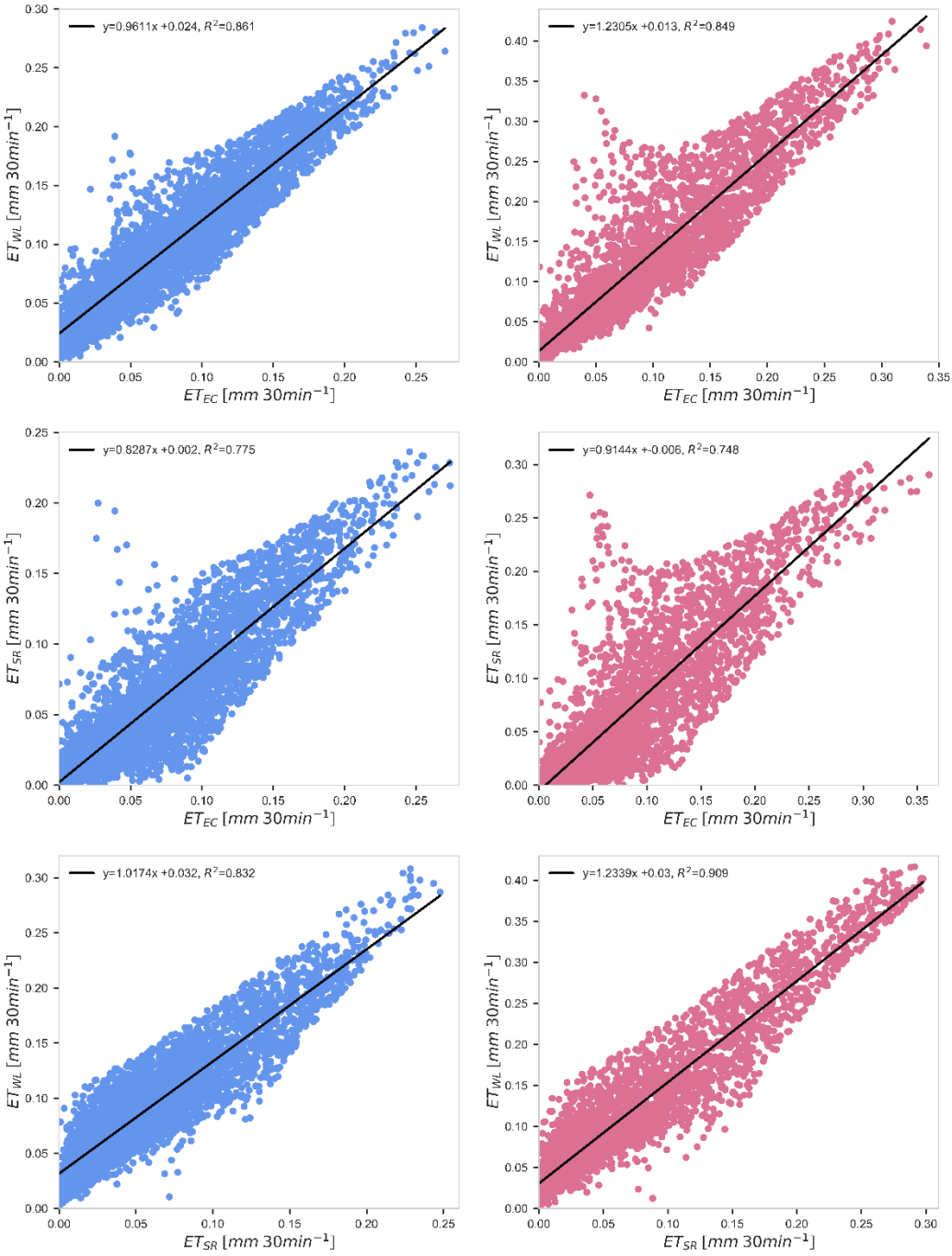

Figure 9. Least-squared linear regression plots comparing sub-daily evapotranspiration estimations for ET_{EC} vs ET_{WL}, ET_{EC} vs ET_{SR}, and ET_{WL} vs ET_{SR} for BAR (blue data points) and RIP (pink data points).

There was also strong agreement between the daily estimations derived from the three different methods as shown in Figure 10. While ET_{SR} and ET_{WL} are strongly correlated with ET_{EC}, it is interesting to note that there was weaker correlation when comparing ET_{SR} to $ET_{WL.}$ As seen shown in Table 4, the lowest R^2 values were 0.787 for ET_{EC} vs ET_{SR} in BAR vineyard. The way the SR and WL methods analyze ramp characteristics can lead to different estimates of ET. However, this is the only instance where there is a noticeable difference. RIP did not show weaker correlation for ET_{SR} vs $ET_{WL.}$

Like sub-daily values, daily estimations of ET derived from these models were screened for any potential outliers due to weather conditions and human interventions that may have led to overestimations and/or erroneous measurements. The Cook's Distance outlier detection method was performed, where any data points resulting in a cook's distance greater than the threshold value of 0.011 were deemed potential outliers. As a result, 5.32%, 6.72%, 8.86%, 8.30%, 10.92%, and 12.23% of data were removed from EC vs WL (BAR), EC vs SR (BAR), WL vs SR (BAR), EC vs WL (RIP), EC vs SR (RIP), and WL vs SR (RIP), respectively, due to values that were found to affected by weather adversity and human interventions.

The slopes of the linear regression for the BAR vineyard are consistent between each comparison. This is significant in showing the potential of WL, SR, and EC in producing similar estimations when applying them to water vapor density data. Like the sub-daily plots, WL also yields higher values of ET estimations compared to those from EC in the RIP vineyard. Despite this overestimation, the values are not much greater than those of the EC results.

Table 4. R-squared and root mean square error (RMSE) values for Linear Regression Models comparing daily evapotranspiration estimations using three mathematical models: EC (EC), Surface Renewal (SR), and Wavelet Analysis (WL).

Vineyard Site	Comparison	R^2	RMSE
BAR	EC vs WL	0.845	0.445
	EC vs SR	0.845	0.409
	WL vs SR	0.787	0.456
RIP	EC vs WL	0.926	0.367
	EC vs SR	0.921	0.299
	WL vs SR	0.915	0.371

Daily ET estimations were graphed against the day of the year (DOY) to observe annual trends. As depicted in Figure 11, the daily value trends for EC and WL overlap significantly throughout the year 2022 in both the BAR and RIP vineyards, which further demonstrates the agreement between the two methods. It is important to note that gaps within the yearly trend reflect the removal of spurious data based on Cook's Distance that were observed in both the sub-daily and daily results. There are some disparities between the two models that emerged between days 160 and 250, where WL produced values lower than those of EC. When comparing the two sites, it's noteworthy that the ET values in RIP nearly double those of BAR during the spring and summer months. This discrepancy might be attributed to their distinct climatic profiles and varying vineyard characteristics.

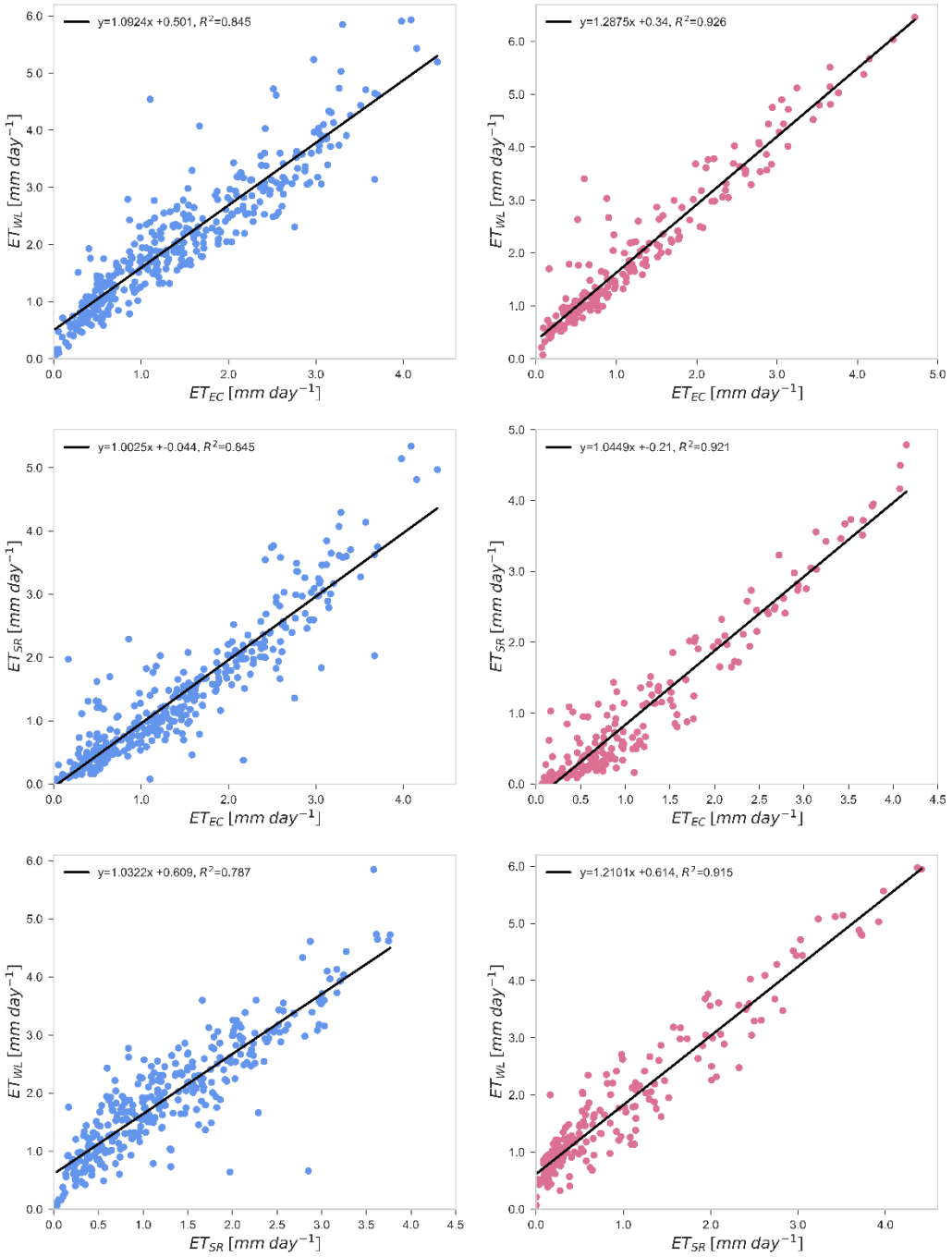

Figure 10. Least-squared linear regression plots comparing daily evapotranspiration estimations for ET_{EC} vs ET_{WL}, ET_{EC} vs ET_{SR}, and ET_{WL} vs ET_{SR} for BAR (blue data points) and RIP (pink data points).

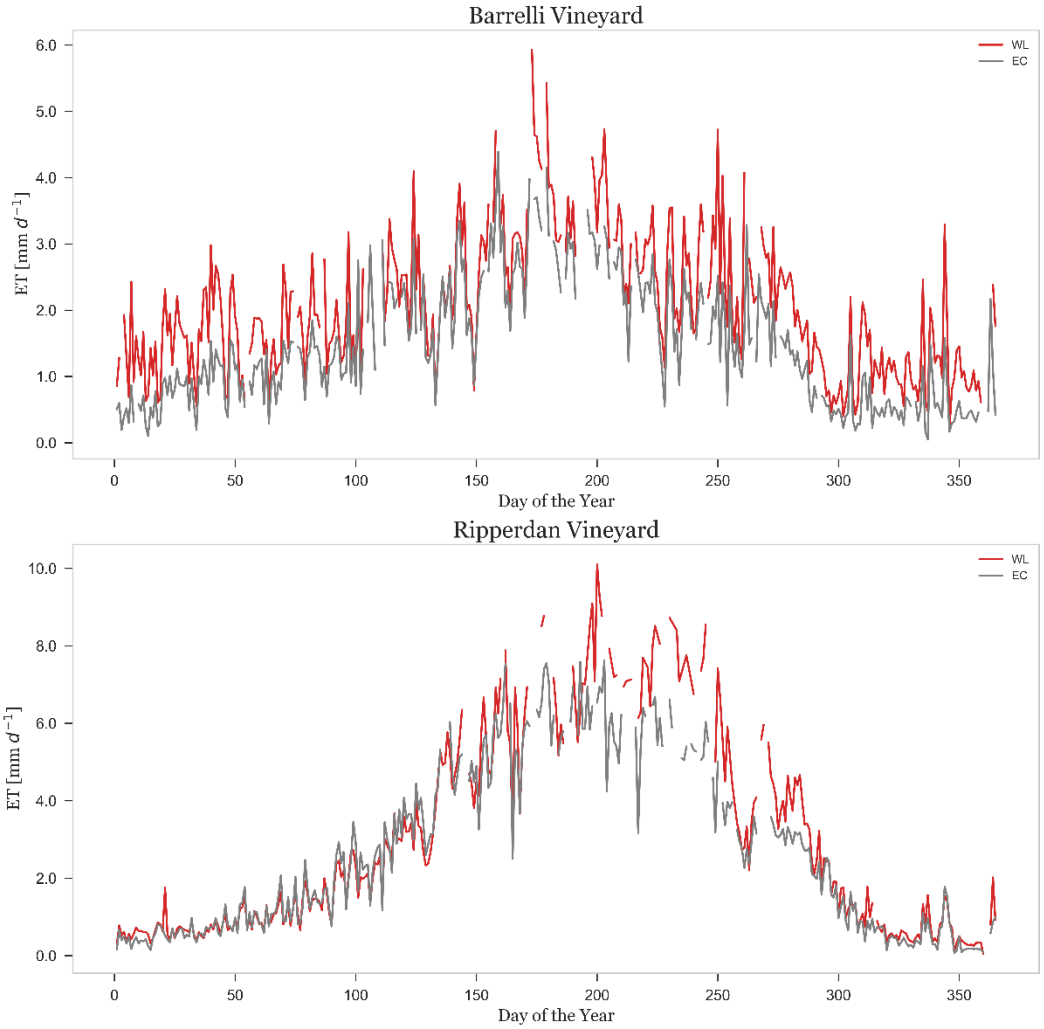

Figure 11. Daily evapotranspiration estimations using Wavelet Analysis (red) and Eddy Covariance (gray) depicted across 2022 for BAR and RIP.

3.3 Sensitivity Analysis Plots

To further understand the robustness of both the WL and SR methods, a sensitivity analysis on frequency was performed. The frequency at which an instrument can measure is a factor in the cost of that instrument. Those that measure at higher frequencies tend to be more expensive than those that measure at lower frequencies. Thus, performing this sensitivity analysis is important in determining if these methods can still reliably estimate ET at lower

frequencies. The main instrument that is used in this study measured the data at 20 Hz. From this dataset, 10 Hz, 5 Hz, and 1 Hz datasets were extracted. Daily ET values were obtained utilizing each of these lower frequency data sets and then compared to the daily ET values obtained with the original 20 Hz data.

Figure 12 illustrates the frequency sensitivity analysis for the BAR vineyard site, where linear regression models were made to compare estimations based on 10 Hz, 5 Hz, and 1 Hz datasets to estimations based on the original 20 Hz data for WL and SR. Visually, there is greater deviation from the linear regression model for SR compared to WL. As frequency decreased, WL showed insignificant changes in both R^2 and RMSE values (Table 5) from 10 Hz (R^2 = 0.995, RMSE = 0.090) to 1 Hz (R^2 = 0.899, RMSE = 0.442). SR also showed insignificant changes, but slightly less changes compared to WL in both R^2 and RMSE values (Table 5) from 10 Hz (R^2 = 0.958, RMSE = 0.201) to 1 Hz (R^2 = 0.912, RMSE = 0.303). Overall, ET estimations at lower frequency show strong correlations with that of higher frequencies for both WL and SR.

Table 5. R-squared and root mean square error (RMSE) values for Linear Regression Models comparing evapotranspiration estimations derived from BAR vineyard's 20 Hz, 10 Hz, 5 Hz, and 1 Hz datasets for Surface Renewal (SR) and Wavelet Analysis (WL).

Method	Comparison	R^2	RMSE
Wavelet Analysis	20 Hz vs 10 Hz	0.995	0.090
	20 Hz vs 5 Hz	0.982	0.189
	20 Hz vs 1 Hz	0.899	0.442
Surface Renewal	20 Hz vs 10 Hz	0.958	0.201
	20 Hz vs 5 Hz	0.961	0.191
	20 Hz vs 1 Hz	0.912	0.303

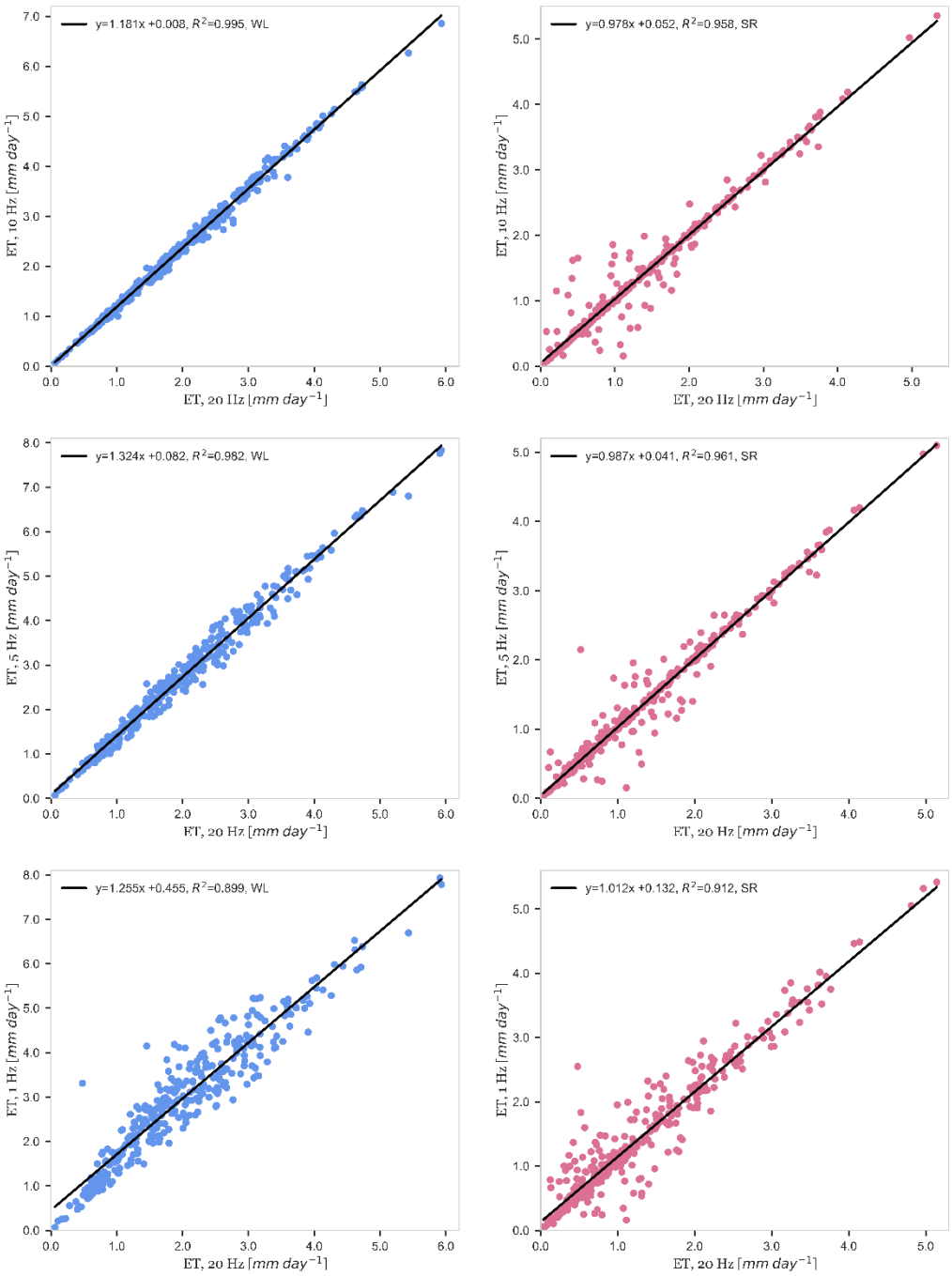

Figure 12. A frequency sensitivity analysis comparing evapotranspiration values derived from wavelet analysis and surface renewal models at different frequencies (20 Hz, 10 Hz, 5 Hz, and 1 Hz) for BAR Vineyard.

Figure 13 illustrates the frequency sensitivity analysis for the RIP vineyard site. Like the BAR vineyard, both SR and WL showed marginal changes in correlation when the frequency decreased from 20 Hz to 1 Hz. WL showed insignificant changes in both R^2 and RMSE values (Table 6) from 10 Hz (R^2 = 0.998, RMSE = 0.077) to 1 Hz (R^2 = 0.956, RMSE = 0.358). While SR showed slightly greater changes in both R^2 and RMSE values (Table 6) from 10 Hz (R^2 = 0.959, RMSE = 0.255) to 1 Hz (R^2 = 0.915, RMSE = 0.368), the estimation yielded between the higher frequency and the lower frequency are very close in value.

Table 6. R-squared and root mean square error (RMSE) values for Linear Regression Models comparing evapotranspiration estimations derived from RIP vineyard's 20 Hz, 10 Hz, 5 Hz, and 1 Hz datasets for Surface Renewal (SR) and Wavelet Analysis (WL).

Method	Comparison	R^2	RMSE
Wavelet Analysis	20 Hz vs 10 Hz	0.998	0.077
	20 Hz vs 5 Hz	0.993	0.157
	20 Hz vs 1 Hz	0.956	0.358
Surface Renewal	20 Hz vs 10 Hz	0.959	0.255
	20 Hz vs 5 Hz	0.963	0.243
	20 Hz vs 1 Hz	0.915	0.368

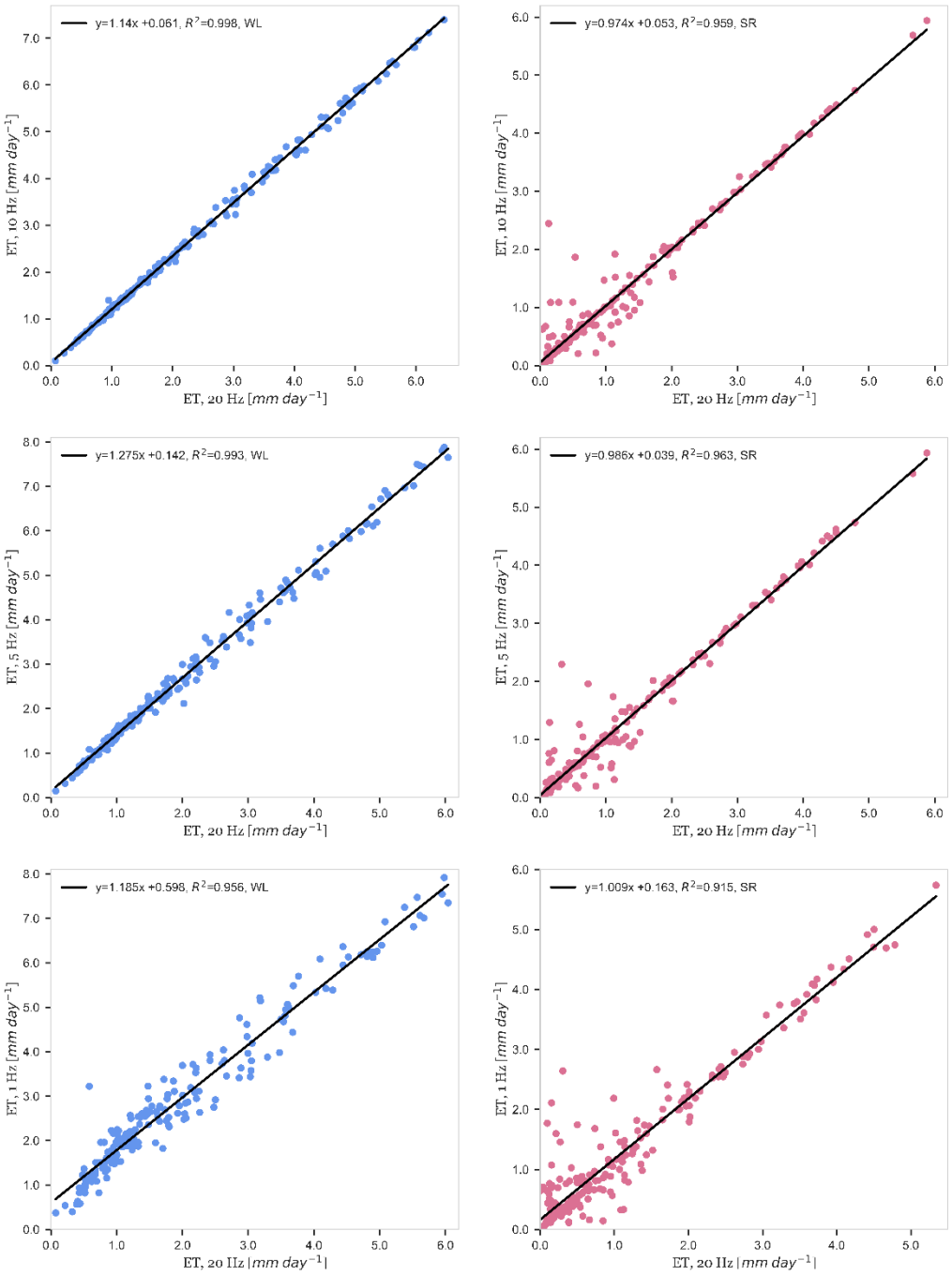

Figure 13. A frequency sensitivity analysis comparing evapotranspiration values derived from wavelet analysis and surface renewal models at different frequencies (20 Hz, 10 Hz, 5 Hz, and 1 Hz) for RIP Vineyard.

4. Discussion

4.1 Alpha Calibration

The α calibration factors can showcase a spectrum of variability depending on a range of diverse factors such as the crop of study, the experimental design, the scalar being measured, the positioning of sensors, and among other considerations (Qui et al., 1995; Snyder et al., 1996; Spano et al., 2000). Regarding factors influencing α values, it is noteworthy to highlight that Paw U et al. (1995) primarily encompassed the application of SR to temperature scalar data proximal to the top of the canopy height. This contrasts with the current study where the observed scalar is water vapor density. Paw U et al. (1995) explained that the role of the α value is to compensate for the nonuniform thermal conditions encountered by air parcels during their traversal within and beyond the canopy. Similarly, this assumption may also be applicable to water vapor density, owing to its inherent non-uniformity within the canopy. In the review by Shapland et al. (2014) that looked at numerous studies involving SR calibration, it was observed that α values may be affected by the canopy's height and the height of measurement. In the present study, the IRGASON® instrument was sited approximately 2.2 meters above the top of the canopy. Based on this observation, our alpha calibration factors may deviate from the expected values. However, the obtained α calibration factors as shown in Figure 8 fall within the expected range for grapevines as derived from a previous study (Spano et al., 2000). The similarity in alpha values between results derived from temperature scalar time series and results derived from water vapor density time series show the potential of water vapor density as an alternative scalar.

The alpha calibration is important for the SR method, as the ET estimations are adjusted using EC results to account for the uneven heating of the air parcels (Paw U et al. 1995). However, the need to calibrate the SR estimations using EC data does not eliminate the use of

the sonic anemometer. Requiring EC data means the necessity of wind data from costly equipment (e.g., sonic anemometer). With the WL method having more flexibility to fit the daughter wavelets to the water vapor data, it was expected that WL would not require the need for an alpha calibration. In this study, WL estimations for ET were not adjusted like the SR estimations before comparing them to EC results. Because WL yielded similar results as that of EC results, it is reasonable to conclude that WL does not require the need to be calibrated and can be a stand-alone method for estimating ET.

4.2 Data Cleaning and Cook's Distance Outlier Determination

The semi-high frequency water vapor density data, collected at a 20 Hz from both BAR and RIP vineyards, contained measurements that were either spurious or missing throughout the entire year. As shown by rolling averages and the Cook's Distance Outlier Determination method, these extreme values (positive or negative), were a result of (1) weather adversities or (2) human interference. Adverse weather conditions, such as wind and rain, played a substantial role, which was expected as previous research done by Castellví et al. (2008) showed that the performance of SR can be compromised due to high humidity. Wind directions ranging from 0° to 90° resulted in winds blowing against the CSAT3S Campbell Scientific Sonic Anemometer's sensor, leading to a reduction in water vapor density data despite the presence of peak daytime temperatures. Conversely, the trend shifted with rainfall. Instances of substantial rainfall or condensation led to an overestimation due to excess water accumulating on the sonic anemometer's surface, often leading to spurious data. Consequently, both the severely underestimated and overestimated data points were disregarded to ensure the accuracy of the final evapotranspiration (ET) estimation.

Human interference, too, emerged as a significant factor. Maintenance of the sonic anemometer requires periodic cleaning, involving distilled water to eliminate dust and dirt from the gas analyzer. However, this intervention occasionally introduced spurious values in the water vapor density data, contributing to inaccuracies. The application of Cook's Distance Outlier Determination highlighted specific days within the year when ET measurements obtained from mathematical methods were disproportionately influenced by strong winds and heavy rain. Predominantly concentrated in the fall and winter months, these outliers aligned with expectations given the elevated levels of precipitation and wind during this period. On the other hand, outliers encountered in the spring and summer months were commonly related to unanticipated wind or rain events and instances of instrument cleaning and maintenance. Furthermore, instances of missing data could be attributed to power outages or systematic sensor issues.

4.3 Agreement between ET_{WL}, ET_{EC}, and ET_{SR}

The sub-daily and daily ET estimations, as presented in Figures 9 and 10, validate the reliability of the Surface Renewal (SR) method for ET measurement. Across all sub-daily and daily estimations, SR exhibited strong agreement with measurements obtained through the EC method, as expected. Numerous studies conducted on various crops, including grass, wheat, sorghum, almonds, and grapevines, have shown analogous agreement between SR and EC methodologies (Spano et al., 2000; Duce et al., 2000). Once more, it is important to acknowledge the distinction in the data being measured. Prior research like Nassar (2021) applied SR onto temperature data, while the current study applied it on water vapor density data. Nevertheless, a noteworthy discovery arises from this this distinction – the proficiency of SR in accurately estimating ET using water vapor density. This achievement may be attributed to the similarity

between "saw-tooth" patterns exhibited by water vapor tracers and those found in temperature data, as observed by Antonia et al. (1979). As previously stated, the core principle of SR, as explained by Paw U et al. (1995), revolves around leveraging these distinct patterns. For temperature data, SR would often rely on the energy balance equation (LE = Rn – G – H; where LE is latent energy, Rn is the net radiation, G is soil heat flux, and H is sensible heat) to calculate the residual energy, which is then converted into ET (Hu et al. 2018; Morán et al., 2020). The distinct advantage of using water vapor density lies in SR's ability to estimate ET without the reliance on the energy balance for residual calculations.

Like SR, the linear regressions comparing sub-daily and daily ET estimates derived using WL demonstrate a strong agreement to that obtained from EC. As shown in Figure 9, 10, and 11, WL can yield reliable estimations of ET. While WL has been successfully applied in studies of precipitation, hydrological fluxes, atmospheric turbulence, ocean wind waves, etc. (Kumar and Foufoula-Georgio, 1997), the application of WL in measuring ET is limited. However, the observation that WL is strongly in agreement with already reliable methods like EC and SR, demonstrates that WL is an alternative method for measuring ET.

4.4 Sensitivity Analysis

The sensitivity analysis has demonstrated the robustness of both WL and SR methods in producing reliable results from lower frequency data sets (10 Hz, 5 Hz, and 1 Hz). Typically, SR and EC rely on semi-high frequency data (10 Hz or 20 Hz) to attain heightened precision in their outcomes (Kustas et al., 2022). However, the associated costs of equipment like the IRGASON® or other similar high-frequency sensors pose a considerable economic hurdle (Paw U et al., 1995). Consequently, the utilization of low-frequency sensors (10 Hz, 5 Hz, and 1Hz) are more cost-effective and emerges as a more advantageous avenue. The sensitivity analysis reveals that

for both WL and SR, the implementation of low-frequency sensors is feasible without compromising the effectiveness and reliability of each method in ET estimation. This not only illustrates the robustness of WL and SR but also paves the way for the exploration of more economically viable methods.

5. Conclusion

The findings in this study highlight the strong performance of WL in estimating ET using water vapor density data. The linear regression models and frequency sensitivity analysis demonstrate that WL exhibits a robust correlation with EC, which is a common practice in tracking biosphere-atmosphere flux interactions, including ET. This strong correlation indicates the reliability of WL in providing accurate ET estimates.

Moreover, the data reveals that WL performs just as well as SR in terms of sub-daily and daily ET estimation and sensitivity to frequency changes. WL showed the ability to yield reliable results even when applied to lower-frequency data. This has significant implications for affordability, as it allows for the use of less expensive instruments that measure at lower frequencies without compromising the accuracy of ET estimates.

The affordability aspect of WL in estimating ET is a crucial advantage. By demonstrating that frequency does not significantly impact the performance of WL, our study suggests that cost-effective instruments measuring at lower frequencies can be employed, making ET monitoring more accessible and cost-efficient. This affordability aspect opens opportunities for a wider range of researchers and practitioners who may have budget constraints but still require accurate ET estimates for their studies or water resource management efforts.

In summary, WL emerges as a reliable and affordable alternative for estimating ET. Its strong correlation with EC, comparable performance to SR, and sensitivity to frequency changes make it a valuable tool for monitoring ET dynamics. The ability to utilize lower-frequency data without compromising accuracy enhances the affordability of ET estimation. Future research should further explore the potential of WL in different environmental contexts and validate its performance against water vapor data collected using more cost-effective instruments.

6. References

Antonia, R. A., Chambers, A. J., Friehe, C. A., & van Atta, C. W. (1979). Temperature Ramps in the Atmospheric Surface Layer. *Journal of the Atmospheric Sciences*, *36*(1), 99–108. https://doi.org/https://doi.org/10.1175/1520-0469(1979)036%3C0099:TRITAS%3E2.0.CO;2

Aubinet, M., Vesala, T., & Papale, D. (2012). *Eddy Covariance: A Practical Guide to Measurement and Data Analysis*. https://doi.org/10.1007/978-94-007-2351-1

Baldocchi, D. D. (2003). Assessing the eddy covariance technique for evaluating carbon dioxide exchange rates of ecosystems: past, present and future. *Global Change Biology*, *9*(4), 479–492. https://doi.org/10.1046/j.1365-2486.2003.00629.x

Baldocchi, D., Finnigan, J., Wilson, K., Paw, K. T., & Falge, E. (2000). ON MEASURING NET ECOSYSTEM CARBON EXCHANGE OVER TALL VEGETATION ON COMPLEX TERRAIN. *Boundary-Layer Meteorology*, *96*, 257–291. http://gaia.agraria.unitus.it/eflux/euro.html

Baldocchi, D. (2014). Measuring fluxes of trace gases and energy between ecosystems and the atmosphere - the state and future of the eddy covariance method. *Global Change Biology*, *20*(12), 3600–3609. https://doi.org/10.1111/gcb.12649

Baldocchi, D. D., Hincks, B. B., & Meyers, T. P. (1988). Measuring Biosphere-Atmosphere Exchanges of Biologically Related Gases with Micrometeorological Methods. *Ecology*, *69*(5), 1331–1340. https://doi.org/https://doi.org/10.2307/1941631

Baldocchi, D., Falge, E., Gu, L., Olson, R., Hollinger, D., Running, S., Anthoni, P., Bernhofer, C., Davis, K., Evans, R., Fuentes, J., Goldstein, A., Katul, G., Law, J. B., Lee, X., Malhi, Y., Meyers, T., Munger, W., Oechel, W., … Hall, H. (2001). FLUXNET: A New Tool to Study the Temporal and Spatial Variability of Ecosystem-Scale Carbon Dioxide, Water Vapor, and Energy Flux Densities. *Bulletin of the American Meteorological Society*, *82*(11), 2415–2434. https://doi.org/https://doi.org/10.1175/1520-0477(2001)082%3C2415:FANTTS%3E2.3.CO;2

Bambach, N., Kustas, W., Alfieri, J., Gao, F., Prueger, J., Hipps, L., McKee, L., Castro, S.J., Alsina, M.M. and McElrone, A.J. (2022). Inter-annual variability of land surface fluxes across vineyards: the role of climate, phenology, and irrigation management. Irrigation Science, 40(4-5), 463-480. https://doi.org/10.1007/s00271-022-00783-1

Brunet, Y., & Collineau, S. (1994). Wavelet Analysis of Diurnal and Nocturnal Turbulence Above a Maize Crop. In *Wavelet Analysis and Its Applications* (Vol. 4, pp. 129–150). https://doi.org/10.1016/B978-0-08-052087-2.50011-6

Burba, G. (2013). *Eddy Covariance Method for Scientific, Industrial, Agricultural and Regulatory Applications: A Field Book on Measuring Ecosystem Gas Exchange and Areal Emission Rates*. https://doi.org/http://dx.doi.org/10.13140/RG.2.1.4247.8561

Castellví, F., Snyder, R. L., & Baldocchi, D. D. (2008). Surface energy-balance closure over rangeland grass using the eddy covariance method and surface renewal analysis. *Agricultural and Forest Meteorology*, *148*(6–7), 1147–1160. https://doi.org/10.1016/j.agrformet.2008.02.012

Chui, C. K. (1992). An Introduction to Wavelets. In *Mathematics of Computation* (Issue 202). JSTOR.

Collineau, S., & Brunet, Y. (1993). Detection of turbulent coherent motions in a forest canopy part I: Wavelet analysis. *Boundary-Layer Meteorology*, *65*, 357–379. https://doi.org/https://doi.org/10.1007/BF00707033

Cook, D. (1977). *Detection of Influential Observation in Linear Regression* (Vol. 19, Issue 1).

Duce, P., Spano, D., Snyder, R.L. and Paw U, K.T. (1997). SURFACE RENEWAL ESTIMATES OF EVAPOTRANSPIRATION. SHORT CANOPIES. *Acta Hortic*. 449, 57-62. https://doi.org/10.17660/ActaHortic.1997.449.6

Foufoula-Georgiou, E., & Kumar, P. (1994). Wavelet Analysis in Geophysics: An Introduction. In *Wavelet Analysis and Its Applications* (Vol. 4, Issue C, pp. 1–43). https://doi.org/10.1016/B978-0-08-052087-2.50007-4

Fox, J. Regression Diagnostics*.* Thousand Oaks, CA: SAGE Publications, Inc., (1991). *Sage Research Methods*, Quantitative Applications in the Social Sciences https://doi.org/10.4135/9781412985604.

Gao, W., Shaw, R. H., & Paw U, K. T. (1989). Observation of organized structure in turbulent flow within and above a forest canopy. *Boundary-Layer Meteorology*, *47*, 349–377. https://doi.org/https://doi.org/10.1007/BF00122339

Gao, W., & Li, B. L. (1993). Wavelet Analysis of Coherent Structures at the Atmosphere-Forest Interface. *Journal of Applied Meteorology and Climatology*, *32*(11), 1717–1725. https://doi.org/https://doi.org/10.1175/1520-0450(1993)032%3C1717:WAOCSA%3E2.0.CO;2

Hu, Y., Buttar, N. A., Tanny, J., Snyder, R. L., Savage, M. J., & Lakhiar, I. A. (2018). Surface Renewal Application for Estimating Evapotranspiration: A Review. In *Advances in Meteorology* (Vol. 2018). Hindawi Limited. https://doi.org/10.1155/2018/1690714

Irmak, S. (2008). Evapotranspiration. In *Encyclopedia of Ecology* (pp. 1432–1438). https://doi.org/https://doi.org/10.1016/B978-008045405-4.00270-6

Kustas, W. P., McElrone, A. J., Agam, N., & Knipper, K. (2022). From vine to vineyard: the GRAPEX multi-scale remote sensing experiment for improving vineyard irrigation management. In *Irrigation Science* (Vol. 40, pp. 435–444). Springer Science and Business Media Deutschland GmbH. https://doi.org/10.1007/s00271-022-00816-9

Lau, K.-M., & Weng, H. (1995). Climate Signal Detection Using Wavelet Transform: How to Make a Time Series Sing. *Bulletin of the American Meteorological Society*, *76*(12), 2391–2402. https://doi.org/https://doi.org/10.1175/1520-0477(1995)076%3C2391:CSDUWT%3E2.0.CO;2

López, A., Ferrero, F., Yangüela, D., Álvarez, C., & Postolache, O. (2017). Development of a computer writing system based on EOG. *Sensors (Switzerland)*, *17*(7). https://doi.org/10.3390/s17071505

McElrone, A. J., Shapland, T. M., Calderon, A., Fitzmaurice, L., Paw U, K. T., Snyder, R. L. (2013). Surface renewal: an advanced micrometeorological method for measuring and processing field-scale energy flux density data. *Journal of Visualized Experiments, 82*. https://doi.org/10.3791/50666

Miralles, D. G., Brutsaert, W., Dolman, A. J., & Gash, J. H. (2020). On the Use of the Term "Evapotranspiration." In *Water Resources Research* (Vol. 56, Issue 11). Blackwell Publishing Ltd. https://doi.org/10.1029/2020WR028055

Morán, A., Ferreyra, R., Sellés, G., Salgado, E., Cáceres-Mella, A., & Poblete-Echeverría, C. (2020). Calibration of the surface renewal method (SR) under different meteorological conditions in an avocado orchard. *Agronomy*, *10*(5). https://doi.org/10.3390/agronomy10050730

Nassar, A., Torres-rua, A., Kustas, W., Alfieri, J., Hipps, L., Prueger, J., Nieto, H., Alsina, M. M., White, W., McKee, L., Coopmans, C., Sanchez, L., & Dokoozlian, N. (2021). Assessing Daily Evapotranspiration Methodologies from one-time-of-day sUAS and EC Information in the GRAPEX project. *Remote Sensing*, *13*(15). https://doi.org/10.3390/rs13152887

Paw U, K. T., Snyder, R. L., Spano, D., & Su, H. B. (2005). Surface renewal estimates of scalar exchange. In *Micrometeorology in Agricultural Systems* (pp. 455–483). wiley. https://doi.org/10.2134/agronmonogr47.c20

Paw U, K. T., Brunet, Y., Collineau, S., Shaw, R. H., Maitani, T., Qiu, J., & Hipps, L. (1992). On coherent structures in turbulence above and within agricultural plant canopies. *Agricultural and Forest Meteorology*, *61*(1–2), 55–68. https://doi.org/https://doi.org/10.1016/0168-1923(92)90025-Y

Paw U, K. T., Qiu, J., Su, H. B., Watanabe, T., & Brunet, Y. (1995). Surface renewal analysis: a new method to obtain scalar fluxes. *Agricultural and Forest Meteorology*, *74*(1–2), 119–137. https://doi.org/10.1016/0168-1923(94)02182-J

Shapland, T. M., Snyder, R. L., Paw U, K. T., & McElrone, A. J. (2014). Thermocouple frequency response compensation leads to convergence of the surface renewal alpha calibration. *Agricultural and Forest Meteorology*, *189–190*, 36–47. https://doi.org/10.1016/j.agrformet.2014.01.008

Snyder, R. L., Spano, D., & Paw, K. T. (1996). Surface renewal analysis for sensible and latent heat flux density. *Boundary-Layer Meteorology*, *77*, 249–266. https://doi.org/https://doi.org/10.1007/BF00123527

Spano, D., Snyder, R. L., Duce, P., & Paw U, K. T. (2000). Estimating sensible and latent heat flux densities from grapevine canopies using surface renewal. *Agricultural and Forest Meteorology*, *104*(3), 171–183. https://doi.org/https://doi.org/10.1016/S0168-1923(00)00167-2

Spano, D., Duce, P., Snyder, R. L., & Paw U, K. T. (1997). Surface renewal estimates of evapotranspiration. Tall canopies. *Acta Horticulturae*, *449*, 63–68. https://doi.org/10.17660/ActaHortic.1997.449.7

Spano, D., Snyder, R. L., Duce', P., & Paw, K. T. (1997). Surface renewal analysis for sensible heat flux density using structure functions. *Agricultural and Forest Meteorology*, *86*(3–4), 259–271. https://doi.org/https://doi.org/10.1016/S0168-1923(96)02420-3

Suvočarev, K., Castellví, F., Reba, M. L., & Runkle, B. R. K. (2019). Surface renewal measurements of H, λE and CO2 fluxes over two different agricultural systems. *Agricultural and Forest Meteorology*, *279*. https://doi.org/10.1016/j.agrformet.2019.107763

Thomas, C., & Foken, T. (2005). Detection of long-term coherent exchange over spruce forest using wavelet analysis. *Theoretical and Applied Climatology*, *80*(2–4), 91–104. https://doi.org/10.1007/s00704-004-0093-0

Van Atta, C. W. (1977). Effect of coherent structures on structure functions of temperature in the atmospheric boundary layer. *Archives of Mechanics*, *29*(1), 161–171.

Verma, S. B. (1990). Micrometeorological methods for measuring surface fluxes of mass and energy. *Remote Sensing Reviews*, *5*(1), 99–115. https://doi.org/10.1080/02757259009532124